ACS OMEGA

Article

Cite This: ACS Omega 2017, 2, 8319−8329

Catalytic Properties of Vanadium Diselenide: A Comprehensive Study on Its Electrocatalytic Performance in Alkaline, Neutral, and Acidic Media

T. Gamze Ulusoy Ghobadi,[†,‡,⊥] Bhushan Patil,[†,‡] Ferdi Karadas,[†,§] Ali K. Okyay,[∥,#] and Eda Yilmaz*[,†,‡]

[†]UNAM−National Nanotechnology Research Center, [‡]Institute of Materials Science and Nanotechnology, [§]Department of Chemistry, and [∥]Department of Electrical and Electronics Engineering, Bilkent University, 06800 Ankara, Turkey

[⊥]Department of Energy Engineering, Faculty of Engineering, Ankara University, 06830 Ankara, Turkey

Supporting Information

ABSTRACT: Here, we report the synthesis of vanadium diselenide (VSe_2) three-dimensional nanoparticles (NPs) and two-dimensional (2D) nanosheets (NSs) utilizing nanosecond pulsed laser ablation technique followed by liquid-phase exfoliation. Furthermore, a systematic study has been conducted on the effect of NP and NS morphologies of VSe_2 in their catalytic activities toward oxygen reduction reaction (ORR), oxygen evolution reaction (OER) and hydrogen evolution reaction (HER) under alkaline, neutral, and acidic conditions. Research on VSe_2 clearly demonstrates that these morphologies do not have a significant difference for ORR and OER; however, a drastic effect of morphology was observed for HER. The ORR activity of both NSs and NPs involves ∼2.85 numbers of electrons with the Tafel slope of 120 mV/dec in alkaline and neutral pH. In alkaline solution, NPs are proved to be an efficient catalyst for OER with an onset potential 1.5 V; however, for HER, NSs have a better onset potential of −0.25 V. Moreover, the obtained NPs have also better catalytic activity with a 400 mV anodic shift in the onset potential compared to NSs. These results provide a reference point for the future application of VSe_2 in energy storage and conversion devices and mass production of other 2D materials.

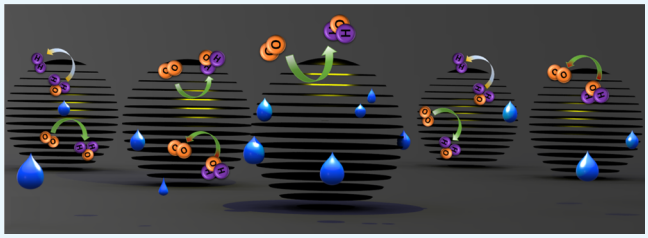

INTRODUCTION

Ultrathin transition-metal dichalcogenides (TMDs) have the general formula MX_2, where M is a transition-metal element (M = Ti, V, Ta, Mo, Re, W) and X is a chalcogen atom (X = S, Se, Te). TMDs are one of the most promising two-dimensional (2D) layered materials[1−3] as next-generation atomically thin devices and have recently become popular due to their unique properties that do not exist in their bulk counterparts.[4,5] MX_2 crystal structure is based on strongly covalent (intralayer) X−M−X bonds within each layer and weak van der Waals (interlayer) X···X interactions between layers.[6] In recent years, broad attention has been paid to employ different types of materials and strategies for hydrogen evolution reaction (HER)[7,8] and oxygen evolution reaction (OER).[9−11] The use of 2D transition-metal compounds in HER[12−14] and OER[8,15] applications has been the subject of many of these studies in recent years. Among all of these 2D TMDs, their semiconducting subsets, where the transition metal is typically Mo or W and the chalcogen atom is made of S or Se, have been the subject of growing attention due to their promising electrical, optoelectrical, and electrochemical characteristics.[16−18]

One of the most frequently employed materials for this application is molybdenum disulfide (MoS_2). It has been found that high catalytic activity of MoS_2 is mainly originated from the high concentration of active sites, which are S sites in this case.[18−24] The hydrogen evolution reaction (HER) activity of this material is found to be linearly correlated with the concentration of these sites.[19] Moreover, it is theoretically demonstrated that the activity of inert basal planes in MoS_2 can be improved by adding different metal atoms, such as Pt, Co, and Ni dopants.[2,25−27] A lot of experimental efforts have been devoted to increase the catalytic performance of the material. The introduction of high concentration of defect sites through the synthesis is one of these approaches. As already mentioned, doping with metal atoms can also enhance the HER activity of the TMD material. Phase transition from semiconductor 2H to metal 1T-MoS_2 was also found as an efficient approach to improve the HER activity.[28−30] The high electrical conductivity originated from metallic behavior in 1T-MoS_2 and 1T-WS_2 layers is supposed to be responsible for its high catalytic activity. However, these 1T products are thermodynamically unfavorable and complicated chemical treatments are required for their synthesis. Unlike these inherently semiconducting group of TMDs that are made of group-six transition metals, group-five TMDs (where the transition metal is V, Nb, and Ta and the chalcogen is S, Se, and Te) are purely metal and can

Received: August 22, 2017
Accepted: November 8, 2017
Published: November 27, 2017

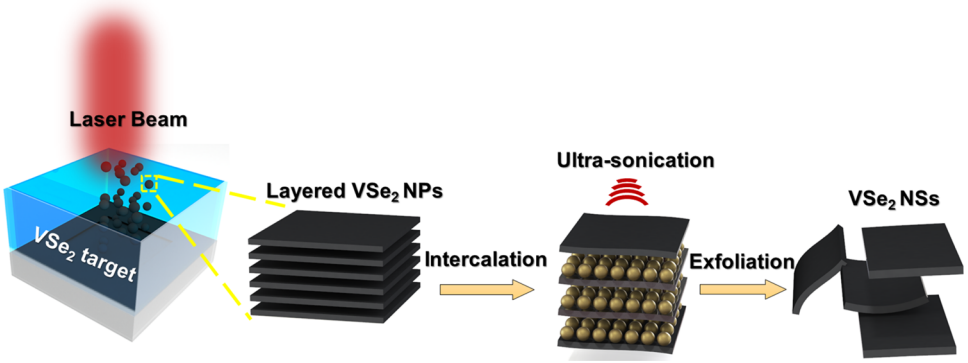

Figure 1. Proposed mechanism for exfoliated VSe_2 NS synthesis: initially, stationary beam was applied to produce VSe_2 NPs and then sonication is applied by adding $LiCO_3$, which results in exfoliation of platelets of VSe_2 NSs.

provide higher electron conductivity.[31−33] Moreover, a high HER activity originating from the high activity of both basal plane and edge sites, having H adsorption free energy approximating to optimal (ΔG_H = 0 eV), has been predicted by the density functional theory for this type of TMDs.[34] In one of the first works, a superior catalytic performance was recorded for single-crystal 1T-VS_2 nanosheets (NSs). The authors demonstrated that this layered TMD design can provide an extremely low overpotential of −68 meV at 10 mA/cm^2, small Tafel slopes (∼34 mV/dec), and high stability demonstrating its potential as a candidate non-noble metal catalyst for HER.[35] Later, a comprehensive study[36] was conducted on the catalytic performance of nine different group-five TMDs, and the findings proved that VTe_2 can have even higher activity compared to VS_2. VTe_2 manifests the lowest HER overpotential at 0.5 V (vs reversible hydrogen electrode (RHE)) and Tafel slope of 55 mV/dec. This difference was actually aroused from the morphology of the synthesized materials. As revealed in a recent study,[37] lithium-exfoliated vanadium dichalcogenides (VS_2, VSe_2, VTe_2) were found to have dramatically different properties from their bulk counterparts. Although the HER catalytic performance of the bulk materials is VTe_2 > VSe_2 > VS_2, the trend for exfoliated materials is VS_2 > VSe_2 > VTe_2. These results together with previous findings suggest that as we move toward a single layer, the VS_2 becomes the most active catalyst and in the bulk phase (thicker nanosheets) VTe_2 is identified as the best-performing material.

Vanadium diselenide (VSe_2) is another member of this group of materials that has attracted a lot of attention as a potential 2D material for future energy storage, conversion, and sensor applications. Besides its intercalation processes[38−40] and highly unusual charge density wave properties,[41] VSe_2 has been predicted to have strong potential to be used as a catalyst or electrode material in electrochemical hydrogen evolution reaction,[42] supercapacitors,[43] photocatalytic reaction,[44] and lithium-ion and sodium-ion batteries.[45−48] However, there have been few studies reported on the electrochemical activities of layered VSe_2.[39,49] Recently, a colloidal synthesis route to obtain single-layer VSe_2 nanosheet has been developed, which offers an excellent HER activity with a low onset overpotential of 108 mV after oxygen plasma exposure.[49] A similar report revealed the potential of VSe_2 for high HER performance.[50] Interestingly, a very recent study proves the application of this material in photoelectrochemical application, which was unexpected before, considering the fact that the VSe_2 is a metallic material with no optical band gap.[44] Essentially, production of monolayer/few-layered typical 2D TMDs is mainly made possible through chemical vapor deposition (CVD)[51] or exfoliation from the bulk. Exfoliation can be applied either in dry phase as a mechanical cleavage[52−54] (the "scotch-tape" method) from bulk crystals or in liquid phase via dispersion in a liquid, served with/without chemical reactions.[55] Although mechanical exfoliation ensures high-quality and micrometer-sized flakes, it is not suitable for large-scale production because the number of layers cannot be controlled precisely.[2] Chemical exfoliation of TMDs, however, is a simple and versatile method to attain nanosheets with high repeatability.[56] This synthesis mainly relies on the lithium-ion-assisted exfoliation and it involves two main mechanisms: (1) permeation of the Li ions into the planar area (intercalation) and (2) breakage of van der Waals bindings using intercalated Li^+ hosts (exfoliation). However, there is still a synthetic challenge to synthesize vanadium diselenide (VSe_2), which belongs to group-five layered dichalcogenides. Over the past few decades, researchers could only realize VSe_2 synthesis by chemical vapor transport,[57−59] chemical vapor deposition (CVD),[51,60] and scotch-tape-based mechanical exfoliation[50] of the bulk VSe_2 until Xu et al.[39] have recently synthesized it in an aqueous solution. Later, other researchers have also proposed different chemical-based synthesis methods to make VSe_2 nanosheets.[49] However, due to the complex chemical environment in solution, it is still challenging to prepare contamination-free samples by a solution-based method.

In the present work, we propose a top-down, large-scale compatible, surfactant-free, and widely adopted approach for the synthesis of VSe_2 nanostructures (directly from bulk) by utilizing a two-stage process. In the first stage, pulsed laser ablation (PLA) technique with stationary beam scanning is applied on the bulk rock to produce VSe_2 nanoparticles (NPs). Following laser ablation, ultrasonication-assisted lithium intercalation process is conducted using lithium carbonate in colloidal solution of NPs to successfully produce VSe_2 nanosheets (NSs). During this process, ultrasonication assists lithium ions to easily permeate into the VSe_2 matrix due to the weak van der Waals interaction between the stacked layers. The experiments are conducted to scrutinize the structural and electrochemical properties of the NP and NS structures. The electrocatalytic activities of VSe_2 NPs and NSs are compared to oxygen evolution reaction (OER), oxygen reduction reaction (ORR), and HER in the alkaline, neutral, and acidic media.

The practical advantage of using neutral solutions is that it is beneficial for the devices that are operated at a physiological pH, i.e., biological and enzymatic fuel cells.[61,62] For this aim,

DOI: 10.1021/acsomega.7b01226
ACS Omega 2017, 2, 8319−8329

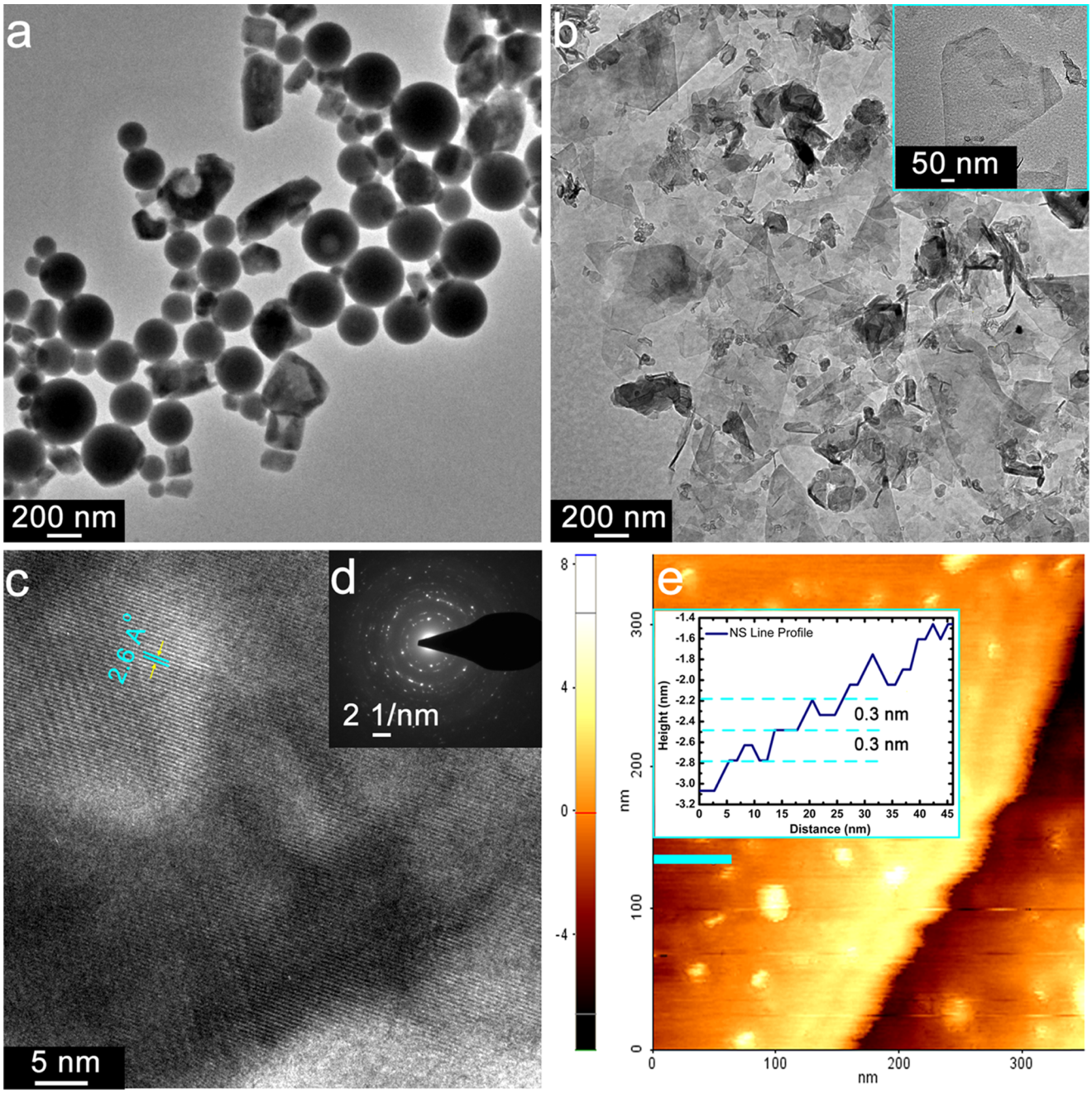

Figure 2. TEM images of (a) VSe_2 NPs obtained by nanosecond laser ablation and (b) VSe_2 NSs after exfoliation (inset shows a magnified image of single NS); (c) HRTEM image of VSe_2 indicating 2.6 Å lattice fringes, with the inset (d) showing the selected area electron diffraction (SAED) pattern; and (e) atomic force microscopy (AFM) topographic image of exfoliated NS with depth profile.

the catalytic behavior of VSe_2 was evaluated under neutral conditions as well. To the best of our knowledge, this is the first report on the fabrication of VSe_2 NPs and NSs by employing laser ablation. Moreover, different from previous studies that are mostly focused on HER performance of the VSe_2, in this study, we have conducted a comprehensive research on the OER and ORR activities of the prepared VSe_2 nanostructures as well.

■ RESULTS AND DISCUSSION

The production of VSe_2 NSs and NPs is schematically depicted in Figure 1. As shown in this figure, first, VSe_2 rock target was ablated in deionized (DI) water to produce NPs with a broad size distribution. To obtain these NPs, the stationary beam was employed for 200 cycles. Afterward, $LiCO_3$ powder was added as a lithium source to this coral-colored solution and the solution was sonicated for 90 min to create NSs, where the solution turns to appear as a darkish transparent solution.

For the initial step, the structural properties of the VSe_2 nanostructures are investigated and shown in Figure 2a−e. The transmission electron microscopy (TEM) images of resultant NPs and NSs confirm that the obtained NPs by laser ablation are nearly three-dimensional (3D) spherical with high size distribution ranging from tens to hundreds of nanometers (as revealed in Figure 2a) and exfoliated layers have ultrathin 2D nature, as clearly observed in Figure 2b. Further investigations

DOI: 10.1021/acsomega.7b01226
ACS Omega 2017, 2, 8319−8329

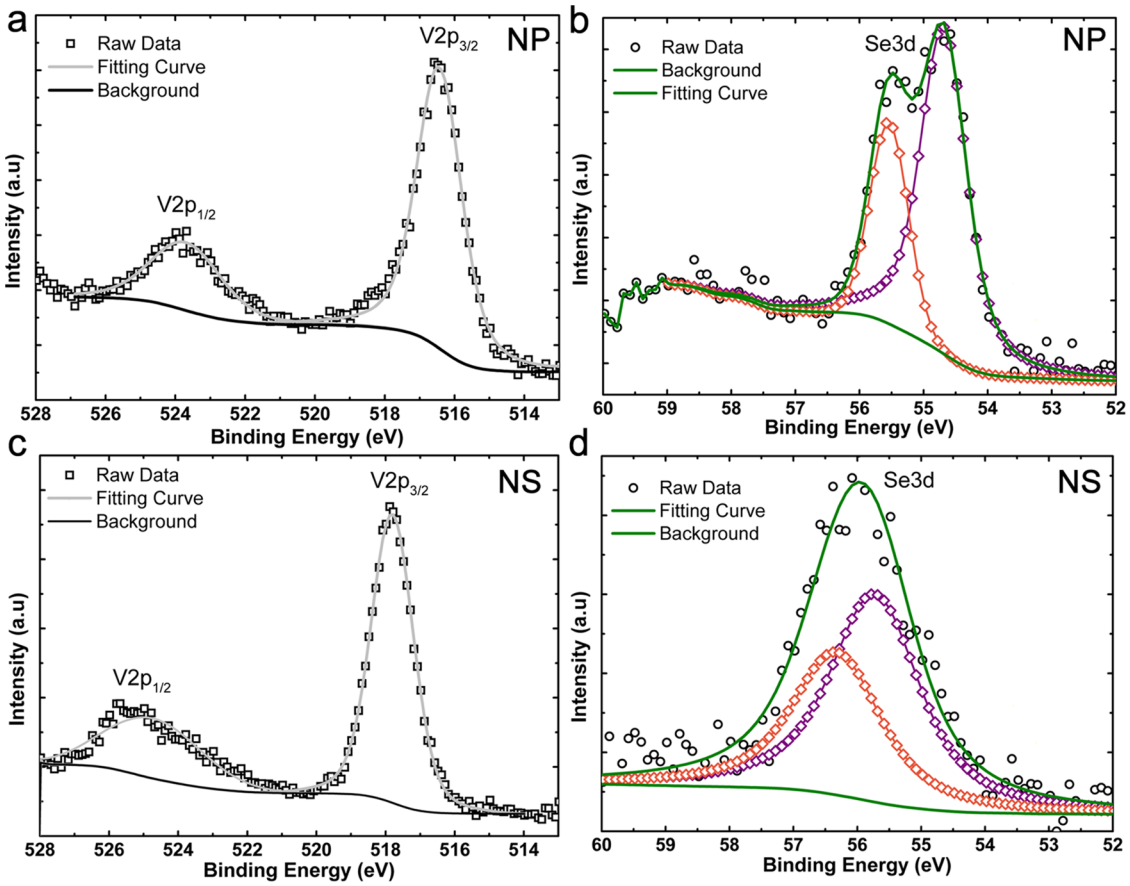

Figure 3. High-resolution XPS and their corresponding fittings: (a) V 2p and (b) Se 3d for VSe_2 NPs, and (c) V 2p and (d) Se 3d for VSe_2 NSs.

using high-resolution TEM (HRTEM) images, shown in Figure 2c, prove that the fabricated NSs are single crystalline, displaying (011) lattice sets with an interplanar spacing of 2.63 Å.

The inset located in the same figure is selected area electron diffraction (SAED) pattern taken from the NS nanostructure, and it displays a typical layered material stacked up by a few/multiple ultrathin sheets. From these images, one can easily understand that upon dropping the VSe_2 single-layer NSs on a substrate it shows an obvious tendency to self-assemble and merge into large sheets. To be more precise, the numbers of VSe_2 layers are investigated by atomic force microscopy (AFM) measurements. The AFM image (Figure 2e) depicts the general observation on the exfoliated layered nature of the nanosheets and the number of layers are studied by probing the thickness; the inset shows a step profile, where the thickness of the layer increases from ∼0.3 nm (estimated thickness of the VSe_2 monolayer) to 2 nm.

For further investigations of NSs, powder X-ray diffraction (PXRD) measurements are conducted to clarify the phase and the crystalline structure of the obtained NSs. As shown in Figure S1, the structure shows a single-crystalline profile and a hexagonal phase with a dominant diffraction peak of (011).[47,63] On the other side, the lack of (001) main peak of VSe_2 bulk can be stemmed from the laser ablation technique and we should note that the (001) and (002) peak positions in VSe_2 strongly depend on the type of intercalant.[64] Also, X-ray diffraction spectrum infers that the impurities are due to the presence of lithium carbonate and selenium product in the material.

To have an insight into the surface elemental composition, X-ray photoelectron spectroscopy (XPS) measurements are also carried out. An almost same peak-fitting trend is observed for both samples. Figure 3a,b compares the deconvolution spectra of V 2p for NS and NP morphologies. As shown in Figure 3a, we have two distinguished peaks located at 516.7.3 eV (V $2p_{3/2}$) and 523.84 eV (V $2p_{1/2}$) for NP form of VSe_2. The peak at ∼517 eV indicates the presence of V^{4+} ions, which is +4 oxidation state of vanadium.[65] Figure 3b shows the doublets of Se 3d spectrum, Se $3d_{5/2}$ and Se $3d_{3/2}$ peaks located at ∼55.2 and ∼56.1 eV with a spin−orbit splitting of 0.86 eV,[66,67] as it is expected; however, both V 2p and Se 3d peaks have been slightly shifted toward higher energies in the case of NSs related to the well-known size reduction effect in metals.

As previously discussed in Introduction, TMDs provide excellent catalysts for important reactions in energy conversion and storage applications. However, to the best of our knowledge, up to now, the electrochemistry and catalytic activity of NP and NS morphologies of VSe_2 have not been studied in detail. Therefore, to understand the catalytic behavior at different pHs toward ORR, OER, and HER, we conducted cylic voltammetry (CV)/linear sweep voltammetry (LSV) experiments in 0.1 M KOH, 0.5 M phosphate-buffered saline (PBS) (pH 7.0), and 0.5 M H_2SO_4 solutions.

Oxygen Reduction Reaction (ORR). The ORR catalytic activities of NSs and NPs were analyzed in O_2-saturated alkaline (0.1 M KOH), neutral (0.5 M PBS, pH 7.0), and acidic (0.5 M H_2SO_4) solutions and normalized by N_2-saturated solutions shown in Figures S2−S4. Because NSs and NPs did not show any ORR catalytic activity in H_2SO_4 (data not

DOI: 10.1021/acsomega.7b01226
ACS Omega 2017, 2, 8319−8329

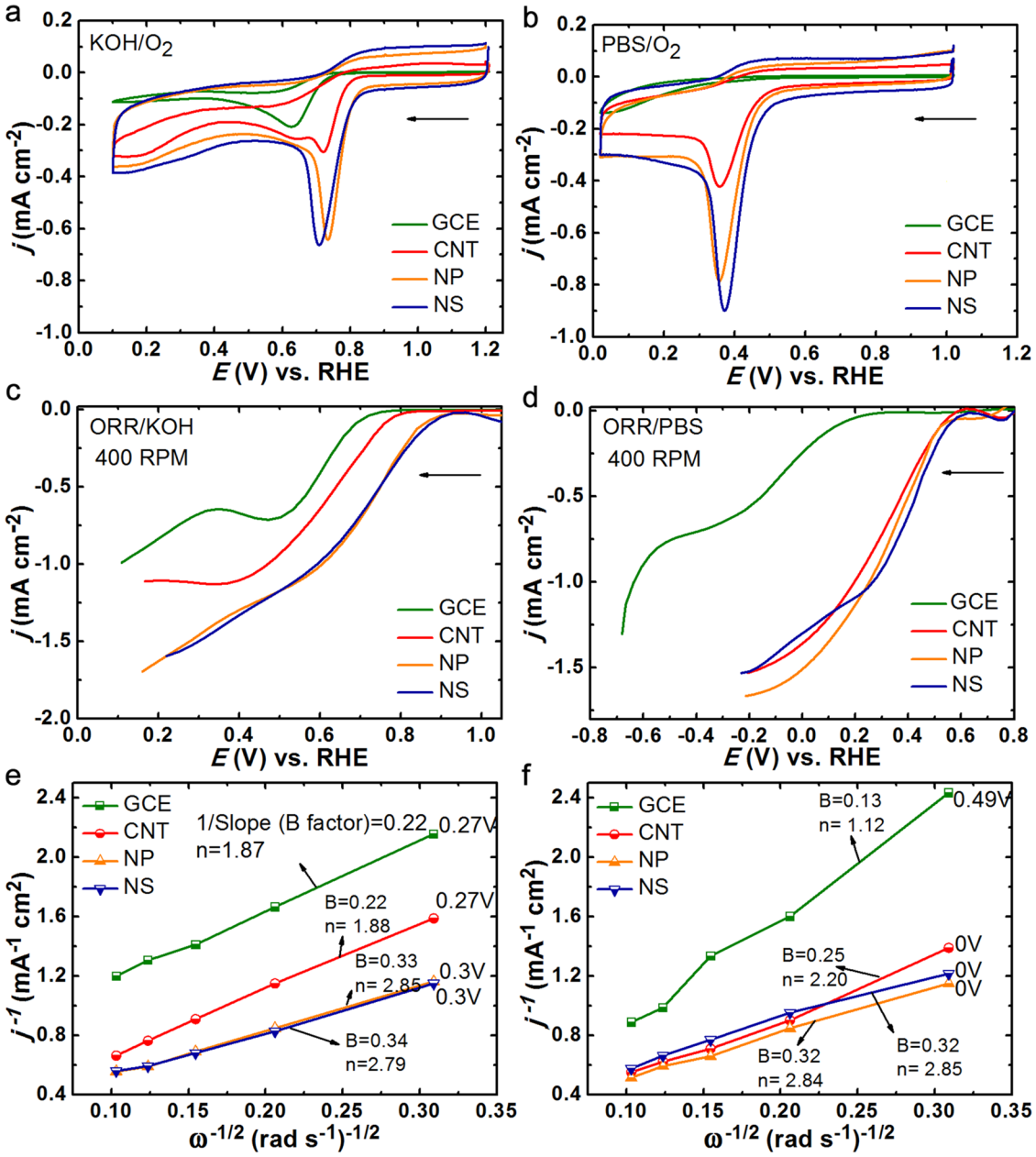

Figure 4. CVs of oxygen reduction obtained at the GCE and CNT, NP, NS catalysts in O_2-saturated (a) 0.1 M KOH solution and (b) 0.5 M solution (pH 7.0); LSV of catalysts at 400 rpm in O_2-saturated (c) 0.1 M KOH solution and (d) 0.5 M PBS solution (pH = 7.0) at 25 °C at a scan rate of 10 mV/s. K–L plots for catalysts in (e) 0.1 M KOH solution and (f) 0.5 M PBS solution (pH 7.0) (data used from Figures S5 and S6).

shown), ORR in alkaline and neutral pHs is reported in this study. The possible reason for the noncatalytic activity of NS and NP in H_2SO_4 might be surface poisoning by sulfate ions.[68−70] The ORR catalytic activities analyzed in KOH and PBS solutions using cyclic voltammograms (CVs) at 10 mV/s scan rate are plotted in Figure 4a,b, respectively. Figure 4a clearly shows an anodic shift in the ORR onset potentials of NS and NP in comparison to carbon nanotubes (CNTs), which are close to the Pt/C in KOH solutions (see Figure S5); however, the onset potentials of NS, NP, and CNT are almost similar as the pH decreased to 7.0 (Figure 4b), indicating the influence of pH on the catalytic activity of VSe_2. Consistent results were obtained in rotating disk electrode (RDE) experiments, as shown in Figure 4c,d. The RDE results at all rotations for the Pt/C, glassy carbon (GC), CNT, NP, and NS catalysts in KOH and PBS are plotted in Figures S5 and S6, respectively. The Tafel slopes obtained at NS and NP cases (from Figure 4c,d) are close to 120 mV/dec, which implies that the first step is a rate-limiting step for the ORR, as shown in Figure S7. Furthermore, the fitting lines in Koutecky–Levich (K–L) catalysts (Figure 4e,f) between j^{-1} and ω^{-1}(where j is the measured limiting current and ω is the electrode rotating rate) are plotted to estimate the number of electrons transferred per oxygen molecule (η) involved in the ORR and related kinetics parameters (for details, see Supporting Information). In the KOH and PBS solutions, the number of electrons involved in the ORR at NS and NP was ∼2.8, which shows that the ORR proceeds through parallel mechanism of two electrons (via H_2O_2 formation) and four electrons (direct reduction to H_2O); however, CNT undergo two-electron ORR through production of H_2O_2. In both KOH and PBS, exchange current density (i_0) and kinetic current density (j_k) values were higher than those of

DOI: 10.1021/acsomega.7b01226
ACS Omega 2017, 2, 8319−8329

Table 1. Typical ORR Results Obtained from GC, CNT, NP, and NS Catalysts Measured in 0.1 M KOH and 0.5 M PBS pH 7.0[a]

catalyst	solution	onset potential/mV	Tafel slope/mV/dec	j_k@0.62 V	i_o	no. of e^- n
Pt/C	KOH	962	120.9	76.72	7.55	3.885
GCE	KOH	700	78.5	0.52	4.08	1.874
CNT	KOH	800	106.2	1.01	4.39	1.884
NP	KOH	932	113.6	4.40	5.56	2.847
NS	KOH	945	106.9	6.80	5.76	2.786
Pt/C	PBS	645				
GCE	PBS	316	191.9	1.99	1.15	1.12
CNT	PBS	545	168	17.14	2.31	2.20
NP	PBS	546	135.4	200	2.46	2.84
NS	PBS	553	124.3	1348	2.64	2.85

[a]All of the potentials were reported versus RHE.

the CNT for NS and NP, providing catalytic activity toward ORR. These results clearly signify that NS and NP morphologies do not have a significant effect on their ORR catalytic activities. Table 1 summarizes the corresponding data for all catalysts. Essentially, the number of electrons involved in the ORR at NP and NS in the alkaline and PBS solution follows parallel ($k_1 = k_2$ and $k_3 = 0$) and serial ($k_2 = 2 \times k_3$ and $k_1 = 0$) pathways shown in Scheme 1.[71] In contrast, ORR at the glassy carbon electrode (GCE) and CNT follows peroxo mechanism and the serial pathway ($k_2 = k_3$ and $k_1 = 0$) favorably with a two-electron process. According to the Sabatier principle, ORR catalytic activity is influenced by the strength of adsorbed reactants, products, or intermediates.[13,72] Thus, ORR catalysis in sulfuric acid, at the NP and NS, might be poor due to strongly adsorbed sulfate ions, which lead to weak interaction with O_2 and intermediates resulting inefficient ORR catalysis.

Scheme 1. ORR Mechanism at GCE, CNT, NP, and NS under KOH and PBS Solutions

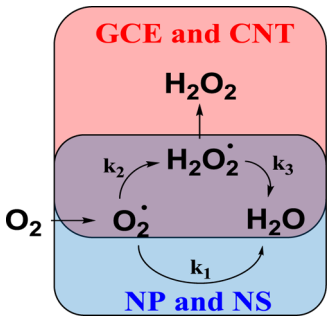

Water Splitting: Oxygen Evolution Reaction (OER) and Hydrogen Evolution Reaction (HER). OER is a four-electron process, and the step of water splitting is generally considered as the major kinetic obstacle of the whole water splitting due to multiple electron transfers during the formation of an O−O bond.[8] Although OER is a thermodynamically reverse process of ORR, change in the liquid to gas phase leads to a different mechanism. Some of the TMDs have already proved to be efficient catalysts for the OER of cobalt, nickel, mixed metal selenides, and so forth.[15] Tahir et. al. reported that surface morphologies can change due to electrochemical treatment.[11] The effect of NS and NP morphologies at different pHs on the OER catalytic activities were realized using KOH, PBS (pH 7.0), and H_2SO_4 solutions. The higher onset potential obtained in OER catalysis of NS and NP in H_2SO_4 than CNT (Figure S8a) could be attributed to surface poisoning of NS and NP in H_2SO_4 solution and thus diminishing of active surface area.

Figure 5 illustrates the water splitting electrocatalytic activity of NSs and NPs in KOH and PBS. The catalytic activity is effective when the reaction is catalyzed at low potential (i.e., onset potentials for OER and HER shift to cathodic and anodic potentials, respectively). Figure 5a clearly shows that the onset potential for OER of NP shifts cathodically by 150 mV in comparison to CNT, whereas NS was similar to CNT. As per convention, the potentials required for different catalysts to deliver a current density of 10 mA/cm^2 ($E_{j=10}$, overpotential value at 10% of an efficient solar water splitting device[73]) are compared and summarized in Table S2. E_j for NP (i.e., 2.49 V) was higher than the superior state-of-the-art OER catalyst IrO_2 with E_j = 1.58 V. Although OER is catalyzed at the NP surface, it has a high Tafel slope of 189 mV/dec (Figure S9 and Table S2), indicating slow kinetics in comparison to IrO_2, but better than CNT. In the PBS solution, both the NSs and NPs are not efficient catalysts because onset potential is more anodic than that obtained for CNT (Figure 5b). On the basis of these results, it can be hypothesized that OH^- ions are necessary for OER catalysis of NPs.

The HER performance of catalysts is also assessed at different pHs and summarized in Table S2 in addition to their catalytic activities for OER. As can be seen in the LSV curves (Figure 5c) of VSe_2, NS can perform well as an outstanding HER catalyst in 1.0 M KOH electrolyte with an onset potential of about −250 mV (shown in Table S3), which is not as good as the commercial Pt catalyst (243 mV), however, much better than the CNT having onset potential −760 mV. In addition, NP also shows a similar HER catalytic activity with an onset potential of −260 mV. Therefore, it can be concluded that VSe_2 is an efficient catalyst for HER in alkaline solution. Morphology, however, does not have a significant effect on the catalytic activity in alkaline solution. The onset potential for HER shows little difference for NSs and NPs in PBS (Figure 5d). Interestingly, NPs have been proven to be an efficient HER catalyst in the H_2SO_4 solution, whereas NSs exhibit poor activity for HER with a cathodic onset potential of 400 mV (Figure S8b). This poor catalytic behavior of NS is actually consistent with the previous results,[37] where it is suggested that the degree of exfoliation can drastically affect the HER performance of the catalysts. A possible reason for the lower HER activity of NSs in H_2SO_4 is the fact that sulfate ions have stronger interaction with 2D NSs rather than the 3D NPs; thus, it can be removed more easily at negative potentials on the NP surface than the NS during hydrogen evolution. Thus, the morphology of catalyst plays an important role in selecting

DOI: 10.1021/acsomega.7b01226
ACS Omega 2017, 2, 8319−8329

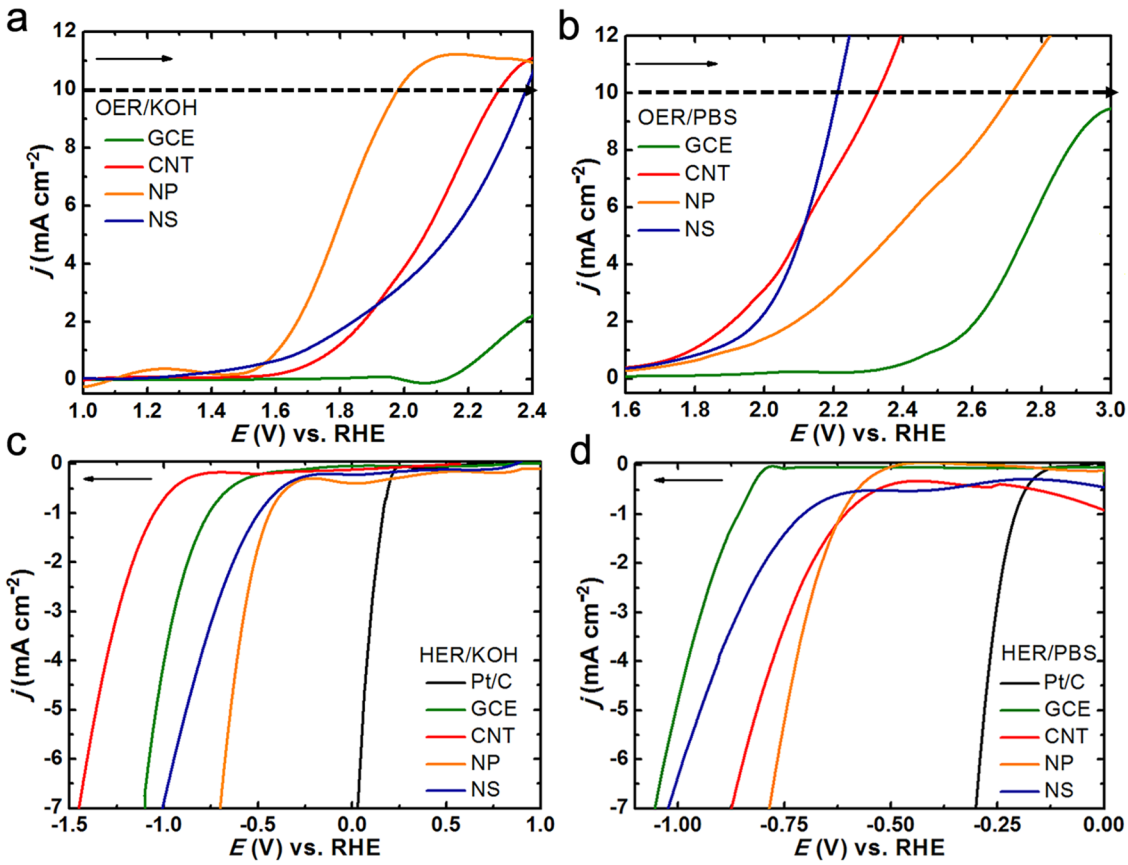

Figure 5. LSVs of OER (a, b) and HER (c, d) in N_2-saturated 0.1 M KOH (a, c) and 0.5 M PBS (pH 7.0) solutions (b, d).

efficient catalyst for HER in acidic media. Revisiting the ORR and OER results, the low catalytic activity in acidic media could be attributed to the poisoning of the catalyst by H^+ and/or SO_4^{2-} ions, which is in line with the HER catalysis results of NS; however, NP confirms its efficient catalytic activity toward HER in H_2SO_4. To be able to evaluate these findings, the HER process should be also revisited. Essentially, the HER reaction can proceed through the Volmer–Tafel (reactions 1 and 2) or Volmer–Heyrovsky mechanism (reactions 1 and 3).[7,12−14,50] As per the nudged elastic band method, HER at TMDs follows the Volmer–Heyrovsky mechanism.[74] Commonly, the first step in the HER at transition-metal selenides proceeds via hydrogen binding to selenium, which creates vacancy via desorption of hydrogen selenide. Thus, hydrogen-binding energy (ΔG_H) and hydrogen selenide binding energy (ΔG_{HS}) are important to realize catalytic activity and its stability.[7]

$$M + H_3O^+ + e^- \rightarrow M - H + H_2O \quad (1)$$

$$2M - H \rightarrow H_2 + M \quad (2)$$

$$M - H + H_3O^+ + e^- \rightarrow H_2 + M + H_2O \quad (3)$$

According to the literature, VSe_2 can exist as metallic TMD in either the 2H trigonal prismatic or 1T octahedral coordination[60,74] and HER can be catalyzed at the basal planes or at the edges. Theoretically, ΔG_{HS} and ΔG_H values at 2H coordination have been reported as −0.57 and 0.62 for basal plane; −0.81 and 0.61 for V-edge; and −0.17 and 0.25 for Se-edge, respectively. Furthermore, ΔG_{HS} and ΔG_H values at 1T coordination are −0.21 and 0.39 for basal plane and −0.17 and 0.25 for edges, respectively.[74] The present study shows that HER was catalyzed at NP and NS in the KOH solution; however, only NP in H_2SO_4 and both morphologies were inactive at neutral pH. Thus, it clearly proves that hydrogen-ion concentration may be one of the causes to change ΔG_{HS}, resulting in HER catalysis being affected by pH. The 2H and 1T coordination influences HER catalytic activity due to the difference in their ΔG_{HS} and ΔG_H values. In the case of NP and NS, the ratio of 2H and 1T might be different, which can be one rational of HER catalysis at NP and inactivity of NS in H_2SO_4 solution. Thus, catalysis in H_2SO_4 can be influenced by sulfate-ion poisoning as well as the difference in the hydrogen-binding energies during the HER.

We further tested the durability of the catalysts by successive CV scanning at a rate of 100 mV/s for 500 cycles. As observed in Figure S10, the VSe_2 NPs and NSs have minor capacitive differences in all three solutions suggesting that they do not dissolve in the solution during cycling and that the overall electrochemically active area remains constant in acidic, alkaline, and neutral pH.

■ CONCLUSIONS

In this work, we conducted a systematic electrochemical analysis on the VSe_2 2D nanosheets and 3D nanoparticles. For this aim, first, we introduced a large-scale-compatible and surfactant-free route to obtain VSe_2 nanoparticles and nanosheets in high yield. In this synthesis, NPs are produced using laser ablation method. Further, we exfoliate them to obtain VSe_2 NSs, using a Li-based intercalation assisted by sonication. In belief, the proposed synthesis method will be equally applicable to other layered TMDs, which can be used for the mass production of 2D nanosheets. Afterward, we performed a

DOI: 10.1021/acsomega.7b01226
ACS Omega 2017, 2, 8319−8329

comprehensive study on the electrochemical properties of the synthesized structures and showed that the electrocatalytic activity depends on the morphology of the catalyst in alkaline, neutral, and acidic mediums. To summarize, the effect of different morphologies is noticeable only in the HER catalytic activities in H_2SO_4 solution. Both the NP and NS show ORR activity in KOH and PBS; however, they are inactive in the H_2SO_4 solution. NP proves to be a competent OER catalyst in KOH, whereas a similar activity is attained by NS in the PBS solution. These results clearly demonstrate that the NS and NP shapes of the VSe_2 catalyst can influence their catalytic activities depending on the pH of solutions. Thus, selection of proper morphology of catalyst is necessary to conclude its catalytic activity toward ORR and water splitting.

■ EXPERIMENTAL SECTION

Chemicals and Reagents. All chemicals were used as received without further purification. Nafion solution (Dupont DE520, 5 wt %), lithium carbonate (Li_2CO_3, 99.99%), and multiwalled carbon nanotubes (MWCNTs) were purchased from Sigma-Aldrich, and VSe_2 crystal rock (>99.995%) was supplied by HQ Graphene. Deionized water (18 MΩ/cm) is used in all experiments.

VSe_2 Nanoparticles (VSe_2 NPs) Synthesis. The PLA technique was modified on the basis of our previously reported method.[75] In brief, a Nufern NuQ fiber laser (NUQA-1064-NA-0030-F1) is operated at ambient temperature with 1064 nm wavelength, 100 ns pulse width duration, 30 kHz pulse repetition rate/frequency, and 1 mJ pulse energy. To synthesize the VSe_2 colloidal nanoparticles, VSe_2 rock is used as a bulk target, which is covered by deionized water, and the water height over the target is adjusted to be ∼1 cm. The laser beam is focused on the VSe_2 target (1 cm diameter active area), immersed in deionized water, with a spot size of about 3.8 mm diameter using a 200 mm focal length taking into account the refraction through the water. The ablation was carried out for 200 loops using the stationary beam (at a fluence amount of 30 mJ/cm^2) to produce nanoparticles with a wide size distribution (10−100 nm).

Lithium Intercalation of VSe_2 Nanosheets (VSe_2NSs). The intercalation reactions were performed by adding 10 mg of Li_2CO_3 into 2 mL of VSe_2 NP solutions, with a molar Li excess of roughly 2:1. Then, the solution was dispersed by ultrasonication for 2 h.

Ink Preparation. The slurries (ink) for RDE measurements were prepared by mixing 8 mg of MWCNT, 60 μL of Nafion solution (5 wt %), 100 μL of ethanol, 500 μL of DI water, and 160 μL of VSe_2 NP or NS solution (∼16 mg) as electrocatalyst. In the absence of VSe_2, ink solutions are prepared by adding the same amount of DI water (160 μL) to the ink solution. Next, the sample was stored for characterization.

Materials Characterization. To characterize the structural properties of the synthesized VSe_2 NPs and NSs, a transmission electron microscope (Tecnai G2-F30, FEI) operated at 200 kV was used. For TEM and high-resolution TEM (HRTEM) measurements, a few droplets of the solution were dispersed on a lacey carbon-coated copper grid. Selected area electron diffraction (SAED) patterns of samples were also collected to understand the growth direction and crystallinity of the prepared nanoparticles. X-ray photoelectron spectroscopy (XPS, Thermoscientific K-Alpha, Al Kα radiation, $h\upsilon$ = 1486.6 eV) measurement was performed at survey mode by operating flood gun to prevent surface charging with the pass energy and step size set to 30 and 0.1 eV, respectively. The peak positions were calibrated by referencing the C 1s peak position (284.8 eV) and shifting other peaks in the spectrum accordingly. Powder X-ray diffraction (PXRD) was carried out by PANalytical X'pert Multi-Purpose Diffractometer, and the patterns were collected in the 2θ range of 10−70° using Bragg−Brentano geometry (Cu Kα radiation). The VSe_2 solutions were drop-cast onto the sheet of thin glass at room temperature. Finally, the height profile and layer thickness were evaluated from the tapping mode atomic force microscopy (AFM, PSIA).

Electrochemical Measurements. Electrochemical measurements were performed using a rotating disk electrode (RDE, SP-150, Bio-Logic Science Instruments) in a standard three-electrode electrochemical cell configuration with catalyst-loaded GCE, Pt spiral wire, and Ag|AgCl|KCl$_{(sat)}$ as the working, counter, and reference electrodes, respectively. For the convenience of comparison, all potentials measured vs Ag|AgCl|KCl$_{(sat)}$ were reported versus RHE and all of the calculations were based on the geometric surface area, unless specified.

The GCE is renewed by polishing with 1 μm diamond particle slurry and then with 0.05 μm alumina powder on the polishing pad. Finally, it is washed ultrasonically with DI water and ethanol for 10 min each and dried at room temperature to make a homogenous film on the GC electrode surface. For performance comparison, the GCE surfaces were investigated in this study by depositing Pt/C, CNT, NP, and NS and comparing with bare GCE. As working electrode, 6 μL of the catalyst ink was loaded on the GCE (3 mm diameter and 0.07068 cm^2 geometric surface area) and dried at room temperature for electrochemical measurements.

The electrochemical measurements were performed in phosphate-buffered saline (PBS, 0.5 M, pH 7.02), potassium hydroxide (0.1 M KOH), and sulfuric acid (0.5 M H_2SO_4) solutions, and prior to each measurement, the electrolyte solution was saturated with either N_2 or O_2 gas (99.999% purity) for 40 min.

Oxygen Reduction Reaction (ORR). Rotating disk electrode (RDE) measurements were performed in an O_2-saturated KOH and PBS solution to assess the ORR activity and kinetics of the Pt/C, GCE, CNT, NP, and NS catalysts with different rotation speeds of 100, 225, 400, 625, and 900 rpm at 25 °C at a scan rate of 10 mV/s.

Water Splitting: Oxygen Evolution Reaction (OER) and Hydrogen Evolution Reaction (HER). The OER and HER catalytic activities of the samples were recorded by LSVs in N_2-saturated 1.0 M KOH, 0.5 M PBS, and 0.5 M H_2SO_4 solutions at a scan rate of 10 mV/s at room temperature.

■ ASSOCIATED CONTENT

Ⓢ Supporting Information

The Supporting Information is available free of charge on the ACS Publications website at DOI: 10.1021/acsomega.7b01226.

Detailed experimental procedures and characterization; XRD image; electrochemical performance measurement results of all electrodes (PDF)

■ AUTHOR INFORMATION

Corresponding Author

*E-mail: yilmaz@unam.bilkent.edu.tr.

DOI: 10.1021/acsomega.7b01226
ACS Omega 2017, 2, 8319−8329

ORCID

T. Gamze Ulusoy Ghobadi: 0000-0002-7669-1587

Present Address

[#]Dr. Okyay was at Bilkent University at the time of the study (A.K.O.).

Author Contributions

The manuscript was written through contributions of all authors. All authors have given approval to the final version of the manuscript.

Notes

The authors declare no competing financial interest.

■ ACKNOWLEDGMENTS

This work was partially supported by the Scientific and Technological Research Council of Turkey (TUBITAK) under Grant No. 115M375. The authors thank Asst. Prof. Serkan Kasirga for supplying material.

■ REFERENCES

(1) Pumera, M.; Sofer, Z.; Ambrosi, A. Layered Transition Metal Dichalcogenides for Electrochemical Energy Generation and Storage. *J. Mater. Chem. A* **2014**, *2*, 8981.

(2) Tedstone, A. A.; Lewis, D. J.; O'Brien, P. Synthesis, Properties, and Applications of Transition Metal-Doped Layered Transition Metal Dichalcogenides. *Chem. Mater.* **2016**, *28*, 1965−1974.

(3) Duan, X.; Wang, C.; Pan, A.; Yu, R.; Duan, X. Two-Dimensional Transition Metal Dichalcogenides as Atomically Thin Semiconductors: Opportunities and Challenges. *Chem. Soc. Rev.* **2015**, *44*, 8859−8876.

(4) Wasey, A. H. M. A.; Chakrabarty, S.; Das, G. P. Quantum Size Effects in Layered VX2 (X = S, Se) Materials: Manifestation of Metal to Semimetal or Semiconductor Transition. *J. Appl. Phys.* **2015**, *117*, No. 064313.

(5) Wang, H.; Yuan, H.; Sae Hong, S.; Li, Y.; Cui, Y. Physical and Chemical Tuning of Two-Dimensional Transition Metal Dichalcogenides. *Chem. Soc. Rev.* **2015**, *44*, 2664−2680.

(6) Lu, T.; Dong, S.; Zhang, C.; Zhang, L.; Cui, G. Fabrication of Transition Metal Selenides and Their Applications in Energy Storage. *Coord. Chem. Rev.* **2017**, *332*, 75−99.

(7) Eftekhari, A. Electrocatalysts for Hydrogen Evolution Reaction. *Int. J. Hydrogen Energy* **2017**, *42*, 11053−11077.

(8) Wang, Y.; Kong, B.; Zhao, D.; Wang, H.; Selomulya, C. Strategies for Developing Transition Metal Phosphides as Heterogeneous Electrocatalysts for Water Splitting. *Nano Today* **2017**, *15*, 26−55.

(9) Eftekhari, A. Tuning the Electrocatalysts for Oxygen Evolution Reaction. *Mater. Today Energy* **2017**, *5*, 37−57.

(10) Anantharaj, S.; Karthick, K.; Kundu, S. Evolution of Layered Double Hydroxides (LDH) as High Performance Water Oxidation Electrocatalysts: A Review with Insights on Structure, Activity and Mechanism. *Mater. Today Energy* **2017**, *6*, 1−26.

(11) Tahir, M.; Pan, L.; Idrees, F.; Zhang, X.; Wang, L.; Zou, J. J.; Wang, Z. L. Electrocatalytic Oxygen Evolution Reaction for Energy Conversion and Storage: A Comprehensive Review. *Nano Energy* **2017**, *37*, 136−157.

(12) Hu, J.; Zhang, C.; Meng, X.; Lin, H.; Hu, C.; Long, X.; Yang, S. Hydrogen Evolution Electrocatalysis with Binary-Nonmetal Transition Metal Compounds. *J. Mater. Chem. A* **2017**, *5*, 5995−6012.

(13) Tao, H.; Gao, Y.; Talreja, N.; Guo, F.; Texter, J.; Yan, C.; Sun, Z. Two-Dimensional Nanosheets for Electrocatalysis in Energy Generation and Conversion. *J. Mater. Chem. A* **2017**, *5*, 7257−7284.

(14) Su, J.; Zhou, J.; Wang, L.; Liu, C.; Chen, Y. Synthesis and Application of Transition Metal Phosphides as Electrocatalyst for Water Splitting. *Sci. Bull.* **2017**, *62*, 633−644.

(15) Wang, M.; Lin, M.; Li, J.; Huang, L.; Zhuang, Z.; Lin, C.; Zhou, L.; Mai, L. Metal−organic Framework Derived Carbon-Confined Ni2P Nanocrystals Supported on Graphene for an Efficient Oxygen Evolution Reaction. *Chem. Commun.* **2017**, *53*, 8372−8375.

(16) Splendiani, A.; Sun, L.; Zhang, Y.; Li, T.; Kim, J.; Chim, C. Y.; Galli, G.; Wang, F. Emerging Photoluminescence in Monolayer MoS2. *Nano Lett.* **2010**, *10*, 1271−1275.

(17) Ganatra, R.; Zhang, Q. Few-Layer MoS2: A Promising Layered Semiconductor. *ACS Nano* **2014**, *8*, 4074−4099.

(18) Zhang, G.; Liu, H.; Qu, J.; Li, J. Two-Dimensional Layered MoS2: Rational Design, Properties and Electrochemical Applications. *Energy Environ. Sci.* **2016**, *9*, 1190−1209.

(19) Jaramillo, T. F.; Jorgensen, K. P.; Bonde, J.; Nielsen, J. H.; Horch, S.; Chorkendorff, I. Identification of Active Edge Sites for Electrochemical H2 Evolution from MoS2 Nanocatalysts. *Science* **2007**, *317*, 100−102.

(20) Li, G.; Zhang, D.; Qiao, Q.; Yu, Y.; Peterson, D.; Zafar, A.; Kumar, R.; Curtarolo, S.; Hunte, F.; Shannon, S.; Zhu, Y.; Yang, W.; Cao, L. All the Catalytic Active Sites of MoS2 for Hydrogen Evolution. *J. Am. Chem. Soc.* **2016**, *138*, 16632−16638.

(21) Yan, Y.; Xia, B.; Ge, X.; Liu, Z.; Wang, J. Y.; Wang, X. Ultrathin MoS2 Nanoplates with Rich Active Sites as Highly Efficient Catalyst for Hydrogen Evolution. *ACS Appl. Mater. Interfaces* **2013**, *5*, 12794−12798.

(22) Wu, Z.; Fang, B.; Wang, Z.; Wang, C.; Liu, Z.; Liu, F.; Wang, W.; Alfantazi, A.; Wang, D.; Wilkinson, D. P. MoS2 Nanosheets: A Designed Structure with High Active Site Density for the Hydrogen Evolution Reaction. *ACS Catal.* **2013**, *3*, 2101−2107.

(23) Benson, J.; Li, M.; Wang, S.; Wang, P.; Papakonstantinou, P. Electrocatalytic Hydrogen Evolution Reaction on Edges of a Few Layer Molybdenum Disulfide Nanodots. *ACS Appl. Mater. Interfaces* **2015**, *7*, 14113−14122.

(24) Ambrosi, A.; Sofer, Z.; Pumera, M. Lithium Intercalation Compound Dramatically Influences the Electrochemical Properties of Exfoliated MoS2. *Small* **2015**, *11*, 605−612.

(25) Deng, J.; Li, H.; Xiao, J.; Tu, Y.; Deng, D.; Yang, H.; Tian, H.; Li, J.; Ren, P.; Bao, X. Triggering the Electrocatalytic Hydrogen Evolution Activity of the Inert Two-Dimensional MoS2 Surface via Single-Atom Metal Doping. *Energy Environ. Sci.* **2015**, *8*, 1594−1601.

(26) Escalera-López, D.; Niu, Y.; Yin, J.; Cooke, K.; Rees, N. V.; Palmer, R. E. Enhancement of the Hydrogen Evolution Reaction from Ni-MoS2 Hybrid Nanoclusters. *ACS Catal.* **2016**, *6*, 6008−6017.

(27) Wang, H.; Tsai, C.; Kong, D.; Chan, K.; Abild-Pedersen, F.; Nørskov, J. K.; Cui, Y. Transition-Metal Doped Edge Sites in Vertically Aligned MoS2 Catalysts for Enhanced Hydrogen Evolution. *Nano Res.* **2015**, *8*, 566−575.

(28) Lukowski, M. A.; Daniel, A. S.; Meng, F.; Forticaux, A.; Li, L.; Jin, S. Enhanced Hydrogen Evolution Catalysis from Chemically Exfoliated Metallic MoS2 Nanosheets. *J. Am. Chem. Soc.* **2013**, *135*, 10274−10277.

(29) Lin, Y.-C.; Dumcenco, D. O.; Huang, Y.-S.; Suenaga, K. Atomic Mechanism of the Semiconducting-to-Metallic Phase Transition in Single-Layered MoS2. *Nat. Nanotechnol.* **2014**, *9*, 391−396.

(30) Leng, K.; Chen, Z.; Zhao, X.; Tang, W.; Tian, B.; Nai, C. T.; Zhou, W.; Loh, K. P. Phase Restructuring in Transition Metal Dichalcogenides for Highly Stable Energy Storage. *ACS Nano* **2016**, *10*, 9208−9215.

(31) Feng, J.; Sun, X.; Wu, C.; Peng, L.; Lin, C.; Hu, S.; Yang, J.; et al. Metallic Few-Layered VS2 Ultrathin Nanosheets: High Two-Dimensional Conductivity for In-Plane Supercapacitors. *J. Am. Chem. Soc.* **2011**, *133*, 17832−17838.

(32) Rout, C. S.; Kim, B.; Xu, X.; Yang, J.; Jeong, H. Y.; Odkhuu, D.; Park, N.; Cho, J.; Shin, H. S. Synthesis and Characterization of Patronite Form of Vanadium Sulfide on Graphitic Layer. *J. Am. Chem. Soc.* **2013**, *135*, 8720−8725.

(33) Jing, Y.; Zhou, Z.; Cabrera, C. R.; Chen, Z. Metallic VS2 Monolayer: A Promising 2D Anode Material for Lithium Ion Batteries. *J. Phys. Chem. C* **2013**, *117*, 25409−25413.

(34) Li, H.; Tsai, C.; Koh, A. L.; Cai, L.; Contryman, A. W.; Fragapane, A. H.; Zhao, J.; Han, H. S.; Manoharan, H. C.; Abild-Pedersen, F.; Nørskov, J. K.; Zheng, X. Activating and Optimizing MoS2 Basal Planes for Hydrogen Evolution through the Formation of Strained Sulphur Vacancies. *Nat. Mater.* **2016**, *15*, 364.

DOI: 10.1021/acsomega.7b01226
ACS Omega 2017, 2, 8319−8329

(35) Yuan, J.; Wu, J.; Hardy, W. J.; Loya, P.; Lou, M.; Yang, Y.; Najmaei, S.; Jiang, M.; Qin, F.; Keyshar, K.; Ji, H.; Gao, W.; Bao, J.; Kono, J.; Natelson, D.; Ajayan, P. M.; Lou, J. Facile Synthesis of Single Crystal Vanadium Disulfi de Nanosheets by Chemical Vapor Deposition for Efficient Hydrogen Evolution Reaction. *Adv. Mater.* **2015**, *27*, 5605−5609.
(36) Chia, X.; Ambrosi, A.; Lazar, P.; Sofer, Z.; Pumera, M. Electrocatalysis of Layered Group 5 Metallic Transition Metal Dichalcogenides (MX2, M = V, Nb, and Ta; X = S, Se, and Te). *J. Mater. Chem. A* **2016**, *4*, 14241−14253.
(37) Wang, Y.; Sofer, Z.; Luxa, J.; Pumera, M. Lithium Exfoliated Vanadium Dichalcogenides (VS2, VSe2, VTe2) Exhibit Dramatically Different Properties from Their Bulk Counterparts. *Adv. Mater. Interfaces* **2016**, *3*, No. 1600433.
(38) Reshak, A. H.; Auluck, S. Theoretical Investigations of the Electronic and Optical Properties of Pure and Alkali Metal Intercalated 1T-VSe2. *Phys. B* **2004**, *349*, 310−315.
(39) Xu, K.; Chen, P.; Li, X.; Wu, C.; Guo, Y.; Zhao, J.; Wu, X.; Xie, Y. Ultrathin Nanosheets of Vanadium Diselenide: A Metallic Two-Dimensional Material with Ferromagnetic Charge-Density-Wave Behavior. *Angew. Chem., Int. Ed.* **2013**, *52*, 10477−10481.
(40) Brauer, H. E.; Ekvall, I.; Olin, H.; Starnberg, H. I.; Wahlström, E.; Hughes, H. P.; Strocov, V. N. Na Intercalation of VSe_2 Studied by Photoemission and Scanning Tunneling Microscopy. *Phys. Rev. B* **1997**, *55*, 10022−10026.
(41) Yadav, C. S.; Rastogi, A. K. Electronic Transport and Specific Heat of 1T-VSe2. *Solid State Commun.* **2010**, *150*, 648−651.
(42) Chhowalla, M.; Shin, H. S.; Eda, G.; Li, L.-J.; Loh, K. P.; Zhang, H. The Chemistry of Two-Dimensional Layered Transition Metal Dichalcogenide Nanosheets. *Nat. Chem.* **2013**, *5*, 263−275.
(43) Marri, S. R.; Ratha, S.; Rout, C. S.; Behera, J. N. 3D Cuboidal Vanadium Diselenide Embedded Reduced Graphene Oxide Hybrid Structures with Enhanced Supercapacitor Properties. *Chem. Commun.* **2017**, *53*, 228−231.
(44) He, S.; Lin, H.; Qin, L.; Mao, Z.; He, H.; Li, Y.; Li, Q. Synthesis, Stability and Intrinsic Photocatalytic Properties of Vanadium Diselenide. *J. Mater. Chem. A* **2017**, *5*, 2163−2171.
(45) Yang, X.; Zhang, Z. Carbon-Coated Vanadium Selenide as Anode for Lithium-Ion Batteries and Sodium-Ion Batteries with Enhanced Electrochemical Performance. *Mater. Lett.* **2017**, *189*, 152−155.
(46) Ōnuki, Y.; Inada, R.; Tanuma, S. I.; Yamanaka, S.; Kamimura, H. Electrochemical Characteristics of TiS2, ZrSe2 and VSe2 in Secondary Lithium Battery. *Jpn. J. Appl. Phys.* **1981**, *20*, 1583−1588.
(47) Wang, Y.; Qian, B.; Li, H.; Liu, L.; Chen, L.; Jiang, H. VSe2/graphene Nanocomposites as Anode Materials for Lithium-Ion Batteries. *Mater. Lett.* **2015**, *141*, 35−38.
(48) Murphy, D. W.; Carides, J. N. Low Voltage Behavior of Lithium/Metal Dichalcogenide Topochemical Cells. *J. Electrochem. Soc.* **1979**, *126*, 349−351.
(49) Zhao, W.; Dong, B. H.; Guo, Z. L.; Su, G.; Gao, R. J.; Wang, W.; Cao, L. X. Colloidal Synthesis of VSe2 Single-Layer Nanosheets as Novel Electrocatalysts for the Hydrogen Evolution Reaction. *Chem. Commun.* **2016**, *52*, 9228−9231.
(50) Yan, M.; Pan, X.; Wang, P.; Chen, F.; He, L.; Jiang, G.; Wang, J.; Liu, J. Z.; Xu, X.; Liao, X.; Yang, J.; Mai, L. Field-Effect Tuned Adsorption Dynamics of VSe2 Nanosheets for Enhanced Hydrogen Evolution Reaction. *Nano Lett.* **2017**, *17*, 4109−4115.
(51) Boscher, N. D.; Blackman, C. S.; Carmalt, C. J.; Parkin, I. P.; Prieto, A. G. Atmospheric Pressure Chemical Vapour Deposition of Vanadium Diselenide Thin Films. *Appl. Surf. Sci.* **2007**, *253*, 6041−6046.
(52) Li, H.; Wu, J.; Yin, Z.; Zhang, H. Preparation and Applications of Mechanically Exfoliated Single-Layer and Multilayer MoS2 and WSe2 Nanosheets. *Acc. Chem. Res.* **2014**, *47*, 1067−107.
(53) Mak, K. F.; Lee, C.; Hone, J.; Shan, J.; Heinz, T. F. Atomically Thin MoS2:A New Direct-Gap Semiconductor. *Phys. Rev. Lett.* **2010**, *105*, No. 136805.
(54) Hollensteiner, S.; Spiecker, E.; Dieker, C.; Jäger, W.; Adelung, R.; Kipp, L.; Skibowski, M. Self-Assembled Nanowire Formation during Cu Deposition on Atomically Flat Vse2 Surfaces Studied by Microscopic Methods. *Mater. Sci. Eng., C* **2003**, *23*, 171−179.
(55) Bernal, M. M.; Álvarez, L.; Giovanelli, E.; Arnáiz, A.; Ruiz-González, L.; Casado, S.; Granados, D.; Pizarro, A. M.; Castellanos-Gomez, A.; Pérez, E. M. Luminescent Transition Metal Dichalcogenide Nanosheets through One-Step Liquid Phase Exfoliation. *2D Mater.* **2016**, *3*, No. 035014.
(56) Zhou, K.-G.; Mao, N.; Wang, H.; Peng, Y.; Zhang, H. A Mixed-Solvent Strategy for Efficient Exfoliation of Inorganic Graphene Analogues. *Angew. Chem., Int. Ed.* **2011**, *50*, 10839−10842.
(57) Nikonov, K. S.; Brekhovskikh, M. N.; Egorysheva, A. V.; Menshchikova, T. K.; Fedorov, V. A. Chemical Vapor Transport Growth of vanadium(IV) Selenide and vanadium(IV) Telluride Single Crystals. *Inorg. Mater.* **2017**, *53*, 1126−1130.
(58) Wiegers, G. A. The Characterisation of VSe2: A Study of the Thermal Expansion. *J. Phys. C: Solid State Phys.* **1981**, *14*, 4225−4235.
(59) Spiecker, E.; Schmid, A. K.; Minor, A. M.; Dahmen, U.; Hollensteiner, S.; Jäger, W. Self-Assembled Nanofold Network Formation on Layered Crystal Surfaces during Metal Intercalation. *Phys. Rev. Lett.* **2006**, *96*, No. 086401.
(60) Zhang, Z.; Niu, J.; Yang, P.; Gong, Y.; Ji, Q.; Shi, J.; Fang, Q.; Jiang, S.; Li, H.; Zhou, X.; Gu, L.; Wu, X.; Zhang, Y. Van Der Waals Epitaxial Growth of 2D Metallic Vanadium Diselenide Single Crystals and Their Extra-High Electrical Conductivity. *Adv. Mater.* **2017**, *29*, No. 1702359.
(61) Shimizu, K.; Sepunaru, L.; Compton, R. G. Innovative Catalyst Design for Oxygen Reduction Reaction for Fuel Cells. *Chem. Sci.* **2016**, *7*, 3364−3369.
(62) Falk, M.; Blum, Z.; Shleev, S. Direct Electron Transfer Based Enzymatic Fuel Cells. *Electrochim. Acta* **2012**, *82*, 191−202.
(63) Gopalakrishnan, J. Insertion/extraction of Lithium and Sodium in Transition Metal Oxides and Chalcogenides. *Bull. Mater. Sci.* **1985**, *7*, 201−214.
(64) Acerce, M.; Voiry, D.; Chhowalla, M. Metallic 1T Phase MoS2 Nanosheets as Supercapacitor Electrode Materials. *Nat. Nanotechnol.* **2015**, *10*, 313−318.
(65) Karamat, S.; Rawat, R. S.; Lee, P.; Tan, T. L.; Ke, C.; Chen, R.; Sun, H. D. Ferromagnetic Signature in Vanadium Doped ZnO Thin Films Grown by Pulsed Laser Deposition. *J. Mater. Res.* **2016**, *31*, 3223−3229.
(66) Cui, Y.; Abouimrane, A.; Lu, J.; Bolin, T.; Ren, Y.; Weng, W.; Sun, C.; Maroni, V. A.; Heald, S. M.; Amine, K. (De)lithiation Mechanism of Li/SeSx (X = 0−7) Batteries Determined by in Situ Synchrotron X-Ray Diffraction and X-Ray Absorption Spectroscopy. *J. Am. Chem. Soc.* **2013**, *135*, 8047−8056.
(67) Zhang, J.; Fan, L.; Zhu, Y.; Xu, Y.; Liang, J.; Wei, D.; Qian, Y. Selenium/interconnected Porous Hollow Carbon Bubbles Composites as the Cathodes of Li-Se Batteries with High Performance. *Nanoscale* **2014**, *6*, 12952−12957.
(68) Saleh, M. M.; Awad, M. I.; Kitamura, F.; Ohsaka, T. Sulphur Dioxide Poisoning and Recovery of Platinum Nanoparticles: Effect of Particle Size. *Int. J. Electrochem. Sci.* **2012**, *7*, 12004−12020.
(69) Hamzehlouyan, T.; Sampara, C.; Li, J.; Kumar, A.; et al. Sulfur Poisoning of a Pt/Al2O3 Oxidation Catalyst: Understanding of SO2, SO3 and H2SO4 Impacts. *Top. Catal.* **2016**, *59*, 1028−1032.
(70) Barbarossa, V.; Brutti, S.; Brunetti, B.; Diamanti, M.; Ricci, G. Study of I-/I2 Poisoning of Fe2O3-Based Catalysts for the H2SO4 Decomposition in the Sulfur-Iodine Cycle for Hydrogen. *Ind. Eng. Chem. Res.* **2009**, *48*, 625−631.
(71) Mishra, R.; Patil, B.; Karadaş, F.; Yılmaz, E. Bioinspired Copper Coordination Polymer Catalysts for Oxygen Reduction Reaction. *ChemistrySelect* **2017**, *2*, 8296−8300.
(72) Rothenberg, B. G. *Catalysis: Concepts and Green Applications*, 2nd ed.; Wiley-VCH Press: Chichester, UK, 2008; p 290.
(73) McCrory, C. C. L.; Jung, S.; et al. Benchmarking Heterogeneous Electrocatalysts for the Oxygen Evolution Reaction. *J. Am. Chem. Soc.* **2013**, *135*, 16977−16987.

DOI: 10.1021/acsomega.7b01226
ACS Omega 2017, 2, 8319−8329

(74) Tsai, C.; Chan, K.; Nørskov, J. K.; Abild-Pedersen, F. Theoretical Insights into the Hydrogen Evolution Activity of Layered Transition Metal Dichalcogenides. *Surf. Sci.* **2015**, *640*, 133−140.
(75) Ulusoy Ghobadi, T. G.; Ghobadi, A.; Okyay, T.; Topalli, K.; Okyay, A. K. Controlling Luminescent Silicon Nanoparticle Emission Produced by Nanosecond Pulsed Laser Ablation: Role of Interface Defect States and Crystallinity Phase. *RSC Adv.* **2016**, *6*, 112520−112526.

DOI: 10.1021/acsomega.7b01226
ACS Omega 2017, 2, 8319−8329